Thin Solid Films 680 (2019) 94–101

Contents lists available at ScienceDirect

Thin Solid Films

journal homepage: www.elsevier.com/locate/tsf

Optical and structural characterization of orthorhombic $LaLuO_3$ using extreme ultraviolet reflectometry

Maksym Tryus[a,g,*], Konstantin V. Nikolaev[b], Igor A. Makhotkin[b], Jürgen Schubert[c,g], Lidia Kibkalo[c,g], Serhiy Danylyuk[d,g], Angelo Giglia[e], Piergiorgio Nicolosi[f], Larissa Juschkin[a,c,g]

[a] Chair for Experimental Physics of Extreme Ultraviolet, RWTH Aachen University, Steinbachstr. 15, 52074 Aachen, Germany
[b] Industrial Focus Group XUV Optics, MESA+ Institute for Nanotechnology, University of Twente, P.O. Box 217, 7500 AE Enschede, Netherlands
[c] Peter Grünberg Institute (PGI-9), Forschungszentrum Jülich GmbH, 52425 Jülich, Germany
[d] Chair for the Technology of Optical Systems, RWTH Aachen University, Steinbachstr. 15, 52074 Aachen, Germany
[e] Italian National Research Council - Istituto Officina Materiali (CNR-IOM), I-34149 Trieste, Italy
[f] Department of Information Engineering, IFN-CNR OUS, University of Padova, via Gradenigo 6B, 35131 Padova, Italy
[g] JARA-FIT - Jülich-Aachen Research Alliance for Fundamentals of Future Information Technology, Forschungszentrum Jülich GmbH, 52425 Jülich, Germany

ARTICLE INFO

Keywords:
Orthorhombic $LaLuO_3$
Optical constants
Extreme ultraviolet reflectometry
Thin films characterization

ABSTRACT

A thin orthorhombic $LaLuO_3$ film, grown on $SrTiO_3$ substrate by pulsed laser deposition, is characterized using multi-angle spectral extreme ultraviolet reflectometry (EUVR). Layer structure parameters and optical constants of $LaLuO_3$ are determined simultaneously by fitting angular reflectivity curves in a wide spectral range (70–200 eV). From near-edge optical constant analysis, La:Lu stoichiometry ratio and the film density are derived. Sample structure is additionally analyzed using XRR, AFM and TEM methods. EUVR as a method of structural characterization is discussed in comparison with XRR. Correlation error analysis of the layer structure parameters, obtained from independent EUVR and XRR fits, is presented.

1. Introduction

Extreme ultraviolet reflectometry (EUVR) allows for non-destructive structural characterization of thin films and layer systems, with determination of their thickness, density and roughness parameters [1–3]. This metrology method is equally applicable to metals and dielectrics, not restricted by the sample conductivity. Due to a very strong and element specific interaction of EUV with matter, especially near absorption edges, EUVR shows high chemical contrast and sensitivity to buried thin interlayers [3–6]. This also makes EUVR suitable for quality control, able to monitor small variations of a nominal sample structure [2]. Spectral reflectance measurements in the near-edge region can provide additional information about the chemical state of the studied material and local coordination environment of its atoms [7–9], while multi-angle approach allows to determine the refractive index of the sample [10–13] with the possibility of depth profiling of the sample composition [14]. In this paper, analytic capabilities of the EUVR technique are demonstrated in application to structural and optical characterization of a 10 nm orthorhombic $LaLuO_3$ sample.

$LaLuO_3$ (LLO), as a high-κ material, presents a useful opportunity for miniaturizing transistor devices. It is exceptionally promising as a future gate dielectric [15,16] due to its high relative permittivity κ (different polymorphs of $LaLuO_3$ exhibit κ-values between 20 and 50 [17–20]). LLO might become the next milestone continuing the progression from SiO_2 ($\kappa = 3.9$) to HfO_2 ($\kappa = 20$), used in industry today [21]. As a rule, ternary oxides show higher permittivity compared to the corresponding binary oxides without a reduction of the band gap [22], which makes $LaLuO_3$ an even more interesting target than either La_2O_3 or Lu_2O_3. Thin orthorhombic films of $LaLuO_3$ raise a particular interest, as they can possess κ-values even higher than 40 [17].

Until present, there was no experimental data available on optical properties of $LaLuO_3$ in EUV. This limits the achievable convergence between the experimental reflectance data and corresponding model-based theoretical calculation, especially in the near-edge region, as only rough values of refractive indices calculated from scattering factors of individual elements can be used. Thus, the accuracy of structural analysis of $LaLuO_3$ samples is restricted. Having a more accurate $LaLuO_3$ optical constants data in EUV would allow for a better sample characterization and quality control of the fabricated films (e. g. for a quick stoichiometry check, possibly even during the growth process). In order to fill this gap and to complement the optical constants database with experimentally obtained EUV refractive indices, multi-angle spectral

* Corresponding author at: Chair for Experimental Physics of Extreme Ultraviolet, RWTH Aachen University, Steinbachstr. 15, 52074 Aachen, Germany
E-mail address: maksym.tryus@rwth-aachen.de (M. Tryus).

https://doi.org/10.1016/j.tsf.2019.04.037
Received 21 September 2018; Received in revised form 5 February 2019; Accepted 22 April 2019
Available online 25 April 2019
0040-6090/ © 2019 Elsevier B.V. All rights reserved.

EUVR measurements have been performed.

2. Experimental details

The studied sample is a 10 nm orthorhombic $LaLuO_3$ film, prepared by the pulsed laser deposition (PLD) method. The target was prepared by sintering a pellet of stoichiometric mixture of the binary metal oxides at 1600 °C. The deposition has been performed on $SrTiO_3$ (100) substrate at 900 °C with oxygen partial pressure of $(1\text{–}5)\times10^{-3}$ mbar. It is an established process that assures epitaxial growth of the orthorhombic LLO modification [17].

Studies of fundamental material properties, such as optical constants determination, require an absolutely calibrated and stable source of EUV radiation. Therefore, the EUVR measurements were carried out at the BEAR beamline of ELETTRA synchrotron [23]. Spectral EUV reflectance of the sample was experimentally measured in the photon energy range of 70–200 eV at different grazing angles of incidence (from 2° to 50° with a step of 3°) in s-polarization (degree of linear polarization - 95%). The energy step was variable (0.1–5 eV), with a more detailed study near the La absorption edge (95–105 eV). However, around 200 eV the larger step was used, thus the absorption edge of Lu at 196.3 eV [24] was not resolved.

The X-ray reflectance (XRR) measurements, presented in this work, were performed on a Philips X'Pert diffractometer with a copper X-ray source at Cu K_α wavelength of 0.154 nm.

3. Theory

The analysis of EUVR data may be performed using available open-access software products, such as IMD [25]. But when it comes to dealing with extensive amounts of data, for instance a combination of spectral and angular EUVR measurements (or a simultaneous analysis of EUVR and XRR data) an alternative approach has to be used. Implemented in MATLAB, it employs the theoretical basis from [26], allowing to analyze a number of reflectivity curves simultaneously.

Direct calculation of the thin film structure that fits to the measured X-ray and EUV reflectivity is impossible due to the known phase problem [27]. However, the data can be analyzed by applying a minimization algorithm (e. g. Levenberg-Marquardt [28]) to the reflectance function, calculated for a given layer system according to the transfer matrix formalism [29] with certain initial assumptions. The reconstructed set of structural and optical layer parameters **p** (which may include thickness, roughness, density, composition and/or refractive index) is found by minimization of the fit goodness value χ^2 [26]. In the context of simultaneous analysis of spectral (λ) and angular (θ) reflectivity data, it has the form:

$$\chi^2 = \frac{1}{L-l}\left[\sum_{\lambda}\sum_{\theta}\frac{\left(I^{\text{calc}}(\lambda,\theta,\mathbf{p}) - I^{\text{exp}}(\lambda,\theta)\right)^2}{\sigma^2(\lambda,\theta)}\right] \tag{1}$$

where L is the total number of data points (spectral and angular) in the experimental EUVR dataset, l is the number of variable parameters p_i in the set **p**, and σ is the uncertainty of the measurement.

On every iteration of the optimization algorithm, the reflectivity of the layer system $I^{\text{calc}}(\lambda,\theta,\mathbf{p})$ is calculated using the transfer matrix method [29] and compared to the experimentally measured value $I^{\text{exp}}(\lambda,\theta)$, according to the above-mentioned χ^2 criterion. The effect of interface roughness/diffuseness is modelled by adding a transition layer that introduces a gradual refractive index change over the interface thickness, according to a sinusoidal (or linear, etc.) profile function [26]. It should be noted that according to this approach, the radiation scattered at the interface roughness (and not captured by the detector) is taken into account indirectly, and diffuse scattering is not considered. Thus the interface thickness reconstructed from EUVR analysis may be effectively larger compared to XRR due to the longer wavelength and correspondingly larger scattering angles.

Stability of a fit result, uncertainty of the obtained fit parameters (p_i) and their correlation can be characterized using the covariance matrix [30]. It is found as the inverse of a matrix constructed by second derivatives (essentially the Hessian) of the calculated reflected intensity, taking into account the experimental uncertainties σ_k. Elements of the above-mentioned Hessian matrix are written as:

$$H_{ij} = \sum_{k=1}^{L}\frac{1}{\sigma_k^2}\frac{\partial^2 I_k^{\text{calc}}}{\partial p_i \partial p_j}. \tag{2}$$

The covariance matrix $\mathbf{C} = \mathbf{H}^{-1}$ is symmetric, and its diagonal elements determine the standard deviations (absolute uncertainties) of structural parameters p_i (they are considered as normally distributed random variables):

$$\Delta p_i = \sqrt{C_{ii}}. \tag{3}$$

The non-diagonal components of the covariance matrix contain the information about correlation of the fit parameters. Correlation of two random variables is defined as the degree of their linear dependency. Covariance elements C_{ij} of structural parameters p_i, p_j, normalized by the product of their standard deviations form the matrix **R** of Pearson's coefficients [28], whose elements have the following form:

$$R_{ij} = \left(\frac{C_{ij}}{\sqrt{C_{ii}C_{jj}}}\right). \tag{4}$$

The elements of matrix **R** are ranging from −1 to 1, making the results easier to interpret and compare. The larger the absolute value of correlation coefficient R_{ij} is, the stronger parameters p_i, p_j are correlated. A positive correlation ($R_{ij} > 0$) means that an increase of parameter p_i can be compensated by an increase of parameter p_j, keeping the same χ^2 value, and vice versa (hence the diagonal symmetry). A negative correlation ($R_{ij} < 0$) in turn implies that a change in χ^2 value caused by an increase of parameter p_i can be compensated by a decrease of parameter p_j.

4. Results and discussion

4.1. Near-edge EUV reflectivity

The experimentally measured EUV reflectance spectra of the sample are presented in Fig. 1 for several angles of grazing incidence. The most notable features of the spectra are: the N_5 absorption edge of La at ~102 eV with the accompanying near-edge fine structure (the oscillations visible from the edge and up to 160 eV) caused by the local surrounding of La atoms (namely Lu and O atoms in the compound).

The strong absorption edge feature at 101.85 ± 0.05 eV is identifiable as arising from La $4d_{5/2}$ electron level. Notably, its position is slightly different from the corresponding tabulated binding energy

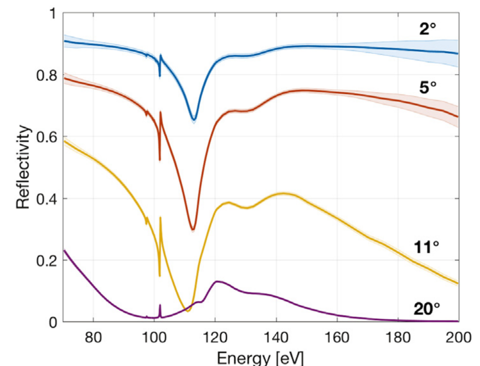

Fig. 1. Exemplary reflectivity spectra of the $LaLuO_3$ sample (with the standard uncertainty), obtained experimentally at different grazing incidence angles in s-polarization.

value (102.5 eV [24]). Furthermore, another discontinuity appears at 97.45 ± 0.05 eV. Its amplitude is rather weak, with only a few data points constituting its shape. The origin of this edge cannot be easily identified, as neither lanthanum or lutetium, nor oxygen actually has electrons with the corresponding binding energy. It is clearly not substrate-related, as it also manifests for the other studied LLO films on a different substrate. Neither can it be readily linked to a contamination, as no element has a tabulated absorption edge at this position: the closest binding energies in the table [24] correspond to Si (99.8 eV, still too far from the observed peak) and Ag (97.0 eV, highly unlikely to be present as a contamination). Possible higher diffraction orders of the monochromator gratings were effectively suppressed by a silicon filter, introduced into the beampath during reflectance measurements below 99 eV. It should be noted that other studied non-LLO samples did not exhibit this feature. On the other hand, an absorption study of free-standing lanthanum nano-films [31] has reported a peak that matches the discussed spectral feature, which makes a strong argument in favor of its La origin.

Looking at the spectral reflectivity curve corresponding to the incidence angle of 20° in Fig. 1, it can be noted that the absorption edge discontinuities transform into pure peaks - features of an absorption spectrum. This is due to the fact that the penetration depth of EUV radiation increases with angle, putting forward the effect of the absorptive part of the LLO refractive index. In fact, changing the angle of incidence allows for a gradual in-depth probing of the layer system. Fig. 2 shows a calculation of the EUV attenuation depth - depth from the surface at which the penetrated radiation intensity is 1/e of the incoming intensity level. It is done by calculating the field distribution within a simple $LaLuO_3/SrTiO_3$ layer model with the same matrix formalism that is used for reflectivity calculation. The attenuation depth is calculated at four angles of incidence, using optical constants obtained from atomic scattering factors [32]. Even though the tabulated scattering factors of La were experimentally obtained [33], they do not contain the sharp structure of the La absorption edges. Apparently, the energy resolution of the measurement in [33] was not sufficient to resolve it. Furthermore, it can be noted that the near-edge oscillations, observed in Fig. 1, being a characteristic of the compound, are not present in the calculation that uses atomic scattering factors (Fig. 2). This highlights the importance of the experimental LLO optical constants data for proper characterization of the film.

4.2. Optical constants determination

Attempting to fit the experimental EUVR spectra using atomic scattering factors as a source of $LaLuO_3$ optical constants (δ, β) strongly limits the fit convergence (Fig. 3a), leading to noticeable discrepancies between the experimental and modelled curves in the near-edge region, where local chemical environment of atoms in the compound plays a major role. However, with the available amount of spectral and angular

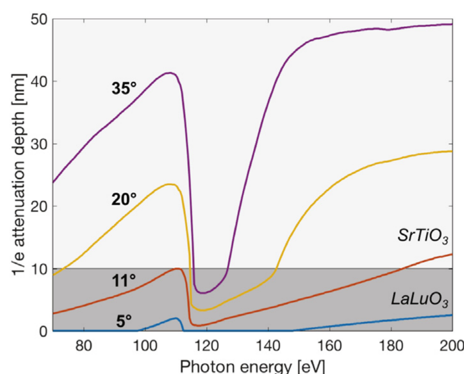

Fig. 2. Calculated attenuation depth of EUV radiation to 1/e of the incoming intensity at different incidence angles for a simple $LaLuO_3/SrTiO_3$ structure.

reflectivity data it is possible to reconstruct the layer structure parameters and the refractive index ($n = 1 - \delta + i\beta$) simultaneously. The result of such a fit is presented in Fig. 3b. It exhibits an order-of-magnitude reduction in the spectral χ^2 value, as compared to the preceding result in Fig. 3a. In both cases, a layer model with carbon on top of the LLO film ($SrTiO_3/LaLuO_3/C$) is used. The presence of an additional overlayer is indicated by the XRR and TEM measurements of the sample (discussed later in Section 4.3), and regarding its composition, carbon contamination as a result of atmospheric exposure and subsequent EUV irradiation seems likely [34,35]. As a matter of fact, adding carbon to the model helps to increase the reflectivity level in the near-edge region, improving the EUVR fit.

The optical constants of the LLO film, obtained from the fit, are presented in Fig. 4 in comparison with the ones calculated from the atomic scattering factors [32] for $LaLuO_3$ density of 8.4 g/cm^3 [36]. The fitted δ and β values, according to the expectations, exhibit the La absorption edge features and near-edge oscillations, discussed in the previous section, not visible in the calculated curves. In addition, a discrepancy of the δ values from the calculation below the La edge (70–100 eV) is observed, while the respective β curve segment is in agreement with the calculation. It can also be noted that the main peak in the β curve around 120 eV and the corresponding valley in the δ curve both have a larger amplitude than the calculated ones. These features are directly connected to the amount of lanthanum in the compound. Subsequently, an increase of the La content above 1 in the calculation, as per $La_xLu_{1-x}O_3$ formula, influences the near-edge section of the optical constants allowing for a better match of the calculated δ & β with the fit results. The density of the compound, on the other hand, serves as a general scaling factor to the δ and β curves over the whole spectral range. The local effect of the La content on the near-edge spectral features allows to estimate the stoichiometric ratio of La:Lu as 1.1:0.9. The density of $La_{1.1}Lu_{0.9}O_3$ in the calculation is unchanged from the value of the bulk $LaLuO_3$ density (8.4 g/cm$_3$), fitting the experimental result quite well.

4.3. Structural characterization

In this section, the sample structure reconstruction, resulting from the EUVR fit in Fig. 3b, is presented. For the purpose of benchmarking, it is compared to XRR fit results, obtained independently, based on the same initial model assumptions.

As the studied LLO sample is a thin 10 nm film, its XRR measurements exhibit interference oscillations attributed to the film thickness (Fig. 5a). However, due to a subtle change in the baseline slope in the backdrop of the oscillations, the experimental data could not be fitted to a single-layer model ($SrTiO_3/LaLuO_3$), indicating the presence of an additional layer on top of the LLO film. XRR technique does not have a strong chemical sensitivity, thus the layer model with a carbon overlayer is employed ($SrTiO_3/LaLuO_3/C$), similar to the EUVR fit. According to the utilized approach, the interface roughness is modelled as an intermixing layer of a certain thickness with a gradual change of the optical constants between the two layers. The best fit result (red line) shows almost no discrepancies from the experimental data, as confirmed by the standardized residuals (st. residual(i) = residual(i)/σ(i), where σ(i) is the corresponding experimental uncertainty for a given data point). A fit of the same data, obtained with GenX software [37], is shown for comparison. GenX uses a different approach to the interface roughness modelling, which is based on the Névot-Croce factors [38]. The GenX fit result (black line) also reproduces the measurement almost perfectly.

In order to compare the layer structure parameters obtained by fitting the EUVR and XRR data, an illustration showing the profiles of the X-ray scattering length density (SLD) with depth are constructed (Fig. 5b): $\mathrm{Re(SLD)} = 2\pi\delta(z)/\lambda^2$. They are calculated at the wavelength of the XRR measurement (0.154 nm) using X-ray atomic scattering factors. The interfaces are modelled according to the corresponding

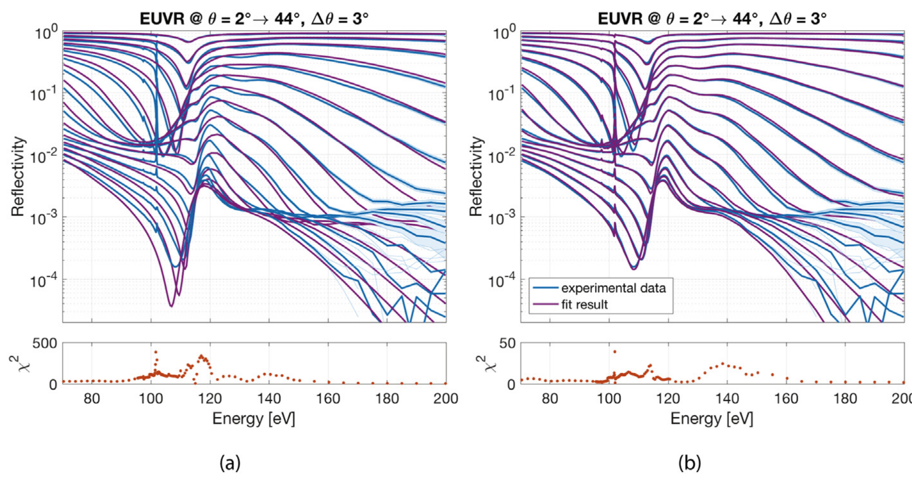

Fig. 3. EUVR fit result (with corresponding χ^2 values) at different grazing incidence angles (from 2° to 44°, step 3° - curves from top to bottom): (a) obtained using LLO optical constants calculated from atomic scattering factors; (b) with LLO optical constants as fit parameters. Spectral χ^2 values are calculated using eq. 1, with summation over θ only.

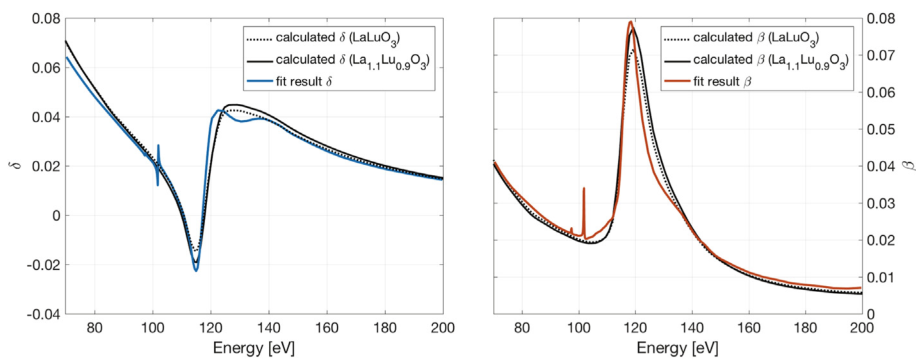

Fig. 4. Comparison of the EUV optical constants (δ & β) obtained from the fit with those calculated using atomic scattering factors for two different stoichiometry ratios (LLO density used in both cases is 8.4 g/cm^3). Standard uncertainty of the fit result falls within the line thickness.

roughness representation, mentioned above. In GenX, a built-in SLD simulation tool is used.

The first observation that can be made from the discussed plot is that the LLO surface profile (together with the carbon layer) has nearly the same overall width in the EUVR (purple solid line) and XRR (red solid line) results. This width is in agreement with the peak-to-valley surface roughness value (~4.5 nm), provided by AFM analysis, indicating that the carbon contamination is non-uniform. A discrepancy between the EUVR and XRR results in the surface profile reconstruction could be caused by different areas of measurement, taking into account the above-mentioned non-uniformity of the contamination layer and a possible LLO film thickness gradient, inherent to the PLD technique of sample fabrication. The XRR fit result from GenX (gray dotted line) is quite similar to the other XRR result, however, providing a larger density and roughness of the surface layer, possibly due to a different modelling approach. Focusing on the substrate/LLO interface, it can be noted that its width is larger in the EUVR result, compared to both XRR results. In fact, an EUVR fit does not converge if the substrate roughness parameter is fixed equal to the result of the XRR fit, meaning that the other structure parameters cannot compensate for the effect of the substrate/LLO interface. This fact did not allow to obtain a combined EUVR + XRR fit for this sample. The observed interface width discrepancy could be attributed to the different influence of scattering in EUV and X-Ray regions, as mentioned in Section 3, or it might be an indication of a density/stoichiometry gradient at the beginning of the LLO growth process, overlooked by the XRR.

TEM (transmission electron microscopy) measurements of the discussed LLO sample are shown in Fig. 6. The lighter shade of a transition

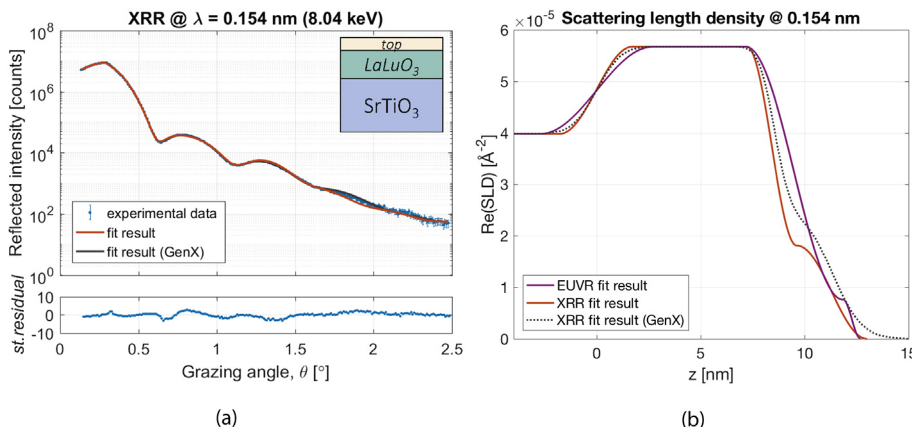

Fig. 5. (a) XRR fit result (with standardized residuals) for 10 nm orthorhombic LLO sample; a fit done on the same structure in GenX is shown for comparison. (b) Distribution profiles of the X-ray scattering length density with depth, obtained from the XRR (Fig. 5a) and EUVR (Fig. 3b) fits. The zero is set in the middle of the substrate/LLO interface.

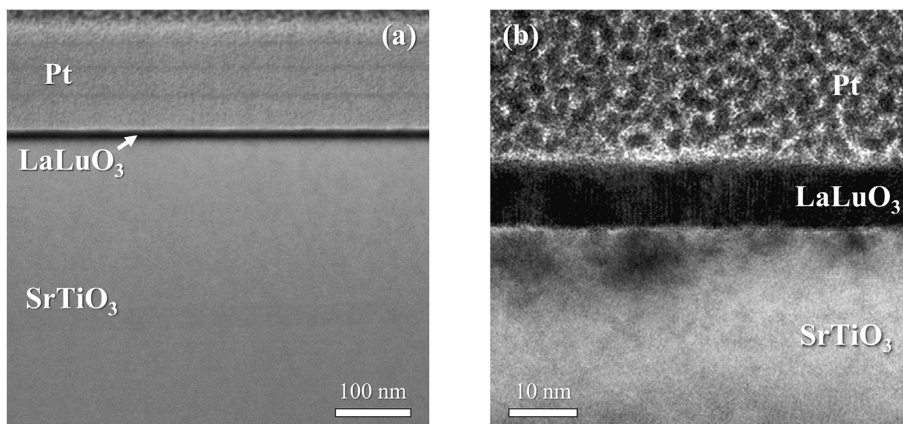

Fig. 6. (a) Scanning TEM bright-field image of 10 nm orthorhombic LLO sample (low magnification); (b) TEM image of the sample (high magnification).

between the LLO and the auxiliary layer of platinum can indicate the presence of a less dense material (e. g. carbon), supporting the conclusions of the EUVR and XRR analysis. At high magnification (Fig. 6b), the roughness of the transition layer becomes noticeable. Also, adjacent to the LLO film, dark areas in the substrate are visible. Among other things, they might indicate substrate strain that manifests through non-uniformities in the substrate density. However, in order to confirm this statement, an additional complex study is needed, which is beyond the scope of the present work.

4.4. Correlation analysis

Based on the approach presented in Section 3, the EUVR and XRR fit results (Fig. 3b and 5a) can be analyzed on the subject of uncertainty of the obtained layer structure parameters and their correlation. For the sake of comparison, the LLO optical constants in EUV will be considered known, as if only a layer structure reconstruction was attempted. This allows to include the LLO density to the set of analyzed variables in EUV (as a scaling factor of the used optical constants) and match the number of structure parameters in both EUVR and XRR sets. Fig. 7 shows a comparison of Pearson's correlation matrices and individual standard uncertainties for six layer structure parameters: ρ_C and ρ_{LLO} are the physical densities of the respective layers, d_{LLO} is the thickness of the homogeneous part of the LLO film, whereas σ_C, σ_{LLO} and σ_{sub} are the interface widths, topping the respective layers. The interface profiles were considered sinusoidal, and the substrate density ρ_{sub} was fixed. Hereby, due to a non-uniformity of the carbon contamination, $d_C = 0$.

Firstly, it can be noted that the relative standard uncertainty of all parameters is well under 1%, except for σ_C^{EUVR}. Being less than 2%, it still provides sensitivity to the layer thickness at the sub-nanometer scale. This speaks in favor of precision and stability of both fit results. A larger uncertainty of σ_C in the EUVR fit result might be influenced by the correlations with σ_{LLO} and ρ_C, stronger than for the XRR data. An important result is that σ_{sub} is not correlated with either σ_{LLO} or σ_C, which leads to a conclusion that the effect of substrate roughness cannot be compensated by any top layer roughness. The uncertainties and correlations indicate that there is a certain advantage in determination of σ_{sub} as well as ρ_C and ρ_{LLO} from the EUVR data, but at such a low overall uncertainty level, this difference is insignificant. It can also be noticed, that the correlation coefficient, connecting the two densities, changes the sign between the EUVR and XRR. It can be explained by the effect of secondary maxima of the interference oscillations, which is weaker in EUV, due to a lower number of oscillations seen. Limiting the XRR data to the primary maximum also leads to a negative correlation between the parameter pair. It indicates that the correlations depend strictly on the considered data. They are merely illustrations, characterizing a certain fit result, so any generalizations should be done cautiously.

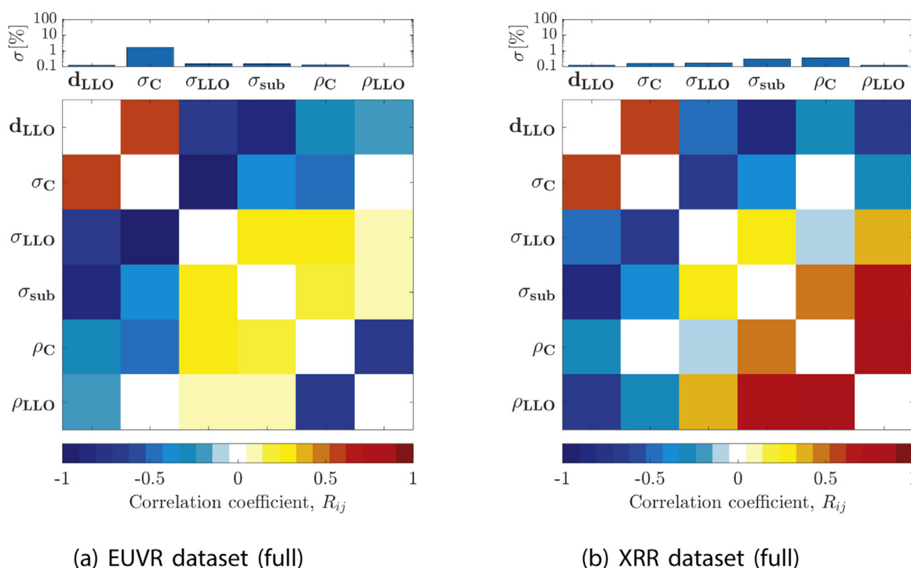

Fig. 7. Correlation matrices of layer structure parameters and their relative uncertainties for the EUVR and XRR fits. Diagonal components are purposefully set to zero.

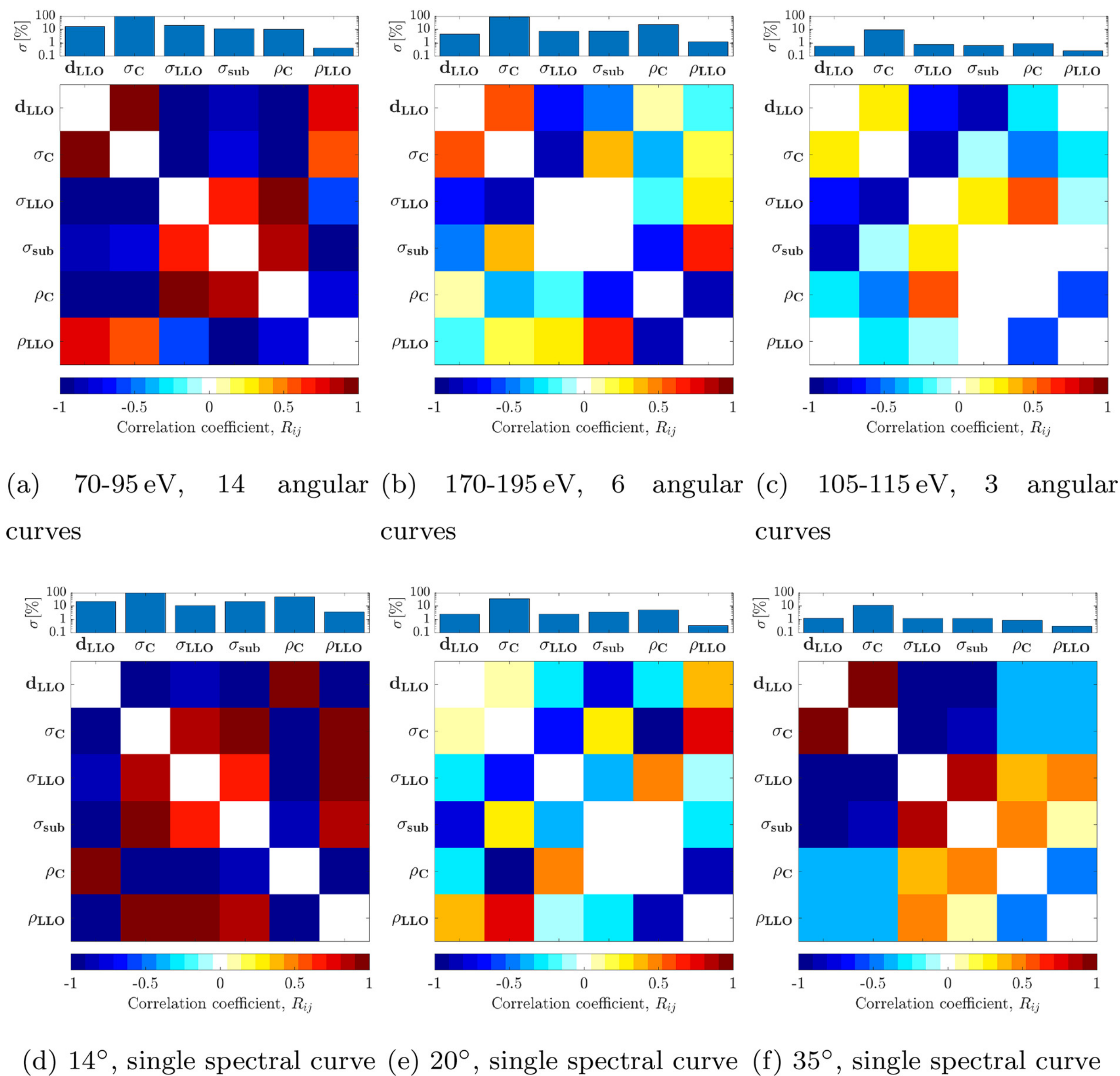

Fig. 8. Correlation matrices of layer structure parameters and their relative uncertainties for the EUVR fit of: (a-c) angular reflectivity curves in different spectral regions; (d-f) spectral reflectivity curves at different grazing angles.

It presents a particular interest to reveal the effect of different angular and spectral regions on the uncertainty and correlation of the layer structure parameters. This will help to optimize the amount of experimental data used for a precise structural reconstruction.

Correlation matrices and relative uncertainties for angular reflectivity data in different spectral regions are shown in Fig. 8 (a–c). The region below the La absorption edges (70–95 eV, Fig. 8a) confines roughly the same total number of datapoints as the XRR measurement (one angular EUVR curve has 15 datapoints). Yet, it exhibits severe correlations of nearly all parameters. Due to a large EUV wavelength in the chosen spectral region (compared to the LLO layer thickness), it contains no oscillations that could decouple heavily correlated structure parameters. Only the LLO density has an acceptable uncertainty value, mainly because it defines the reflectance cut-off at the critical angle, the shape of which was determined quite accurately in the discussed spectral region. Moving towards the higher photon energies (170–195 eV, Fig. 8b), where thickness oscillations become more prominent, improves the correlations, maintaining approximately the same uncertainty level with a smaller dataset. But an even better result can be achieved with only 3 angular curves (45 datapoints total) in the direct vicinity of the absorption edges of La (105–115 eV, Fig. 8c). This spectral range provides the best contrast of the LLO film with the substrate and carbon contamination due to a negative δ value of LLO.

A similar comparison for spectral EUVR data at different incidence angles is presented in Fig. 8 (d–f). Below the critical angle of total external reflection, one spectral curve (169 datapoints) does not contain enough information to reconstruct the layer structure. All parameters are strongly correlated (Fig. 8d), and the relative uncertainties reach up to 100%. The situation can be improved by adding more spectral curves to the dataset, but, more importantly, by moving the angle of incidence past the critical angle (Fig. 8e). Furthermore, with an increase of the grazing angle of incidence, the surface parameters are becoming more correlated (Fig. 8f), which is likely caused by the increased penetration depth of the EUV radiation. It indicates that for every angle of incidence there is a different depth, at which radiation-matter interaction is the most efficient. Attenuation depth, found as the depth still retaining $1/e$ ($\sim 37\%$) of the incoming intensity, might be a suitable criterion for estimation of such sensitivity. Fig. 2 illustrates that below 11° most part of the radiation is confined within the LLO film while at 35° it penetrates deep into to the substrate, which corresponds to the observed

correlations. The correlations can be reduced by attempting multi-angle reflectance measurements, providing a scan of the probing depth with angle. However, it should be noted that correlations are essentially relative (normalized) quantities, thus the primary focus of the analysis should be placed on the absolute values of the covariance elements (i. e. the uncertainties of the fit parameters).

5. Conclusions

Spectral reflectivity of 10 nm orthorhombic $LaLuO_3$ film has been experimentally obtained in the range of 70–200 eV at grazing angles of incidence from 2° to 50° with a step of 3°, using synchrotron EUV radiation. Non-tabulated La absorption edge feature is observed.

By fitting the entire set of angular and spectral reflectance data to a model, it has been possible to obtain the layer structure parameters of the sample and the corresponding optical constants of $LaLuO_3$ film, simultaneously. It has been shown that the stoichiometry of the film ($La_xLu_{1-x}O_3$) has a major effect on the near-edge part of the determined refractive index, allowing to estimate the lanthanum content in the compound.

Structure of the sample has been analyzed using EUVR, XRR, AFM and TEM methods. Distribution profiles of the X-ray SLD with depth, obtained from independent XRR and EUVR fits, are compared and analyzed.

Correlation analysis of the layer structure parameters (such as layer thickness, density and interface width), obtained from the EUVR and XRR fits has been performed, showing the relative uncertainty values not exceeding 2% in both cases. Regarding the optimization of data acquisition in the future EUVR studies, the correlation study indicates that angle-resolved approach presents the greatest potential for the EUVR method, allowing for in-depth probing and more precise reconstruction of layer structures. The wavelength of the EUVR measurement should be selected to provide the best chemical contrast, according to the studied material composition.

Acknowledgements

M.T. acknowledges financial support from the EU FP7 Erasmus Mundus Joint Doctorate Programme EXTATIC under framework partnership agreement FPA-2012-0033. K.V.N. and I.A.M. acknowledge the support of the Industrial Focus Group XUV Optics of the MESA+ Institute for Nanotechnology of the University of Twente, notably the industrial partners ASML, Carl Zeiss SMT GmbH, PANalytical, as well as the Province of Overijssel and the NWO. L.J. acknowledges financial support from the Helmholtz Association for a Helmholtz Professorship (Initiative and Networking Fund).

References

[1] S. Döring, F. Hertlein, A. Bayer, K. Mann, EUV reflectometry for thickness and density determination of thin film coatings, Appl. Phys. A 107 (4) (2012) 795–800, https://doi.org/10.1007/s00339-012-6914-6.

[2] M. Banyay, L. Juschkin, E. Bersch, D. Franca, M. Liehr, A. Diebold, Cross characterization of ultrathin interlayers in HfO2 high-k stacks by angle resolved x-ray photoelectron spectroscopy, medium energy ion scattering, and grazing incidence extreme ultraviolet reflectometry, J. Vac. Sci. Technol. A 30 (4) (2012) 041506, , https://doi.org/10.1116/1.4718433.

[3] M. Nayak, G.S. Lodha, Optical response near the soft X-ray absorption edges and structural studies of low optical contrast system using soft X-ray resonant reflectivity, J. Atomic Mol. Optic. Phys. 2011 (2011) 1–23, https://doi.org/10.1155/2011/649153.

[4] M. Banyay, L. Juschkin, T. Bücker, P. Loosen, A. Bayer, F. Barkusky, S. Döring, C. Peth, K. Mann, H. Blaschke, I. Balasa, D. Ristau, XUV metrology: surface analysis with extreme ultraviolet radiation, Proc. SPIE 7361 (2009) 736113, https://doi.org/10.1117/12.833648.

[5] S. Danylyuk, S. Herbert, P. Loosen, R. Lebert, A. Schäfer, J. Schubert, M. Tryus, L. Juschkin, Multi-angle spectroscopic extreme ultraviolet reflectometry for analysis of thin films and interfaces, Phys. Status Solidi C 12 (3) (2015) 318–322, https://doi.org/10.1002/pssc.201400117.

[6] M.G. Sertsu, M. Nardello, A. Giglia, A.J. Corso, C. Maurizio, L. Juschkin, P. Nicolosi, Analysis of buried interfaces in multilayer mirrors using grazing incidence extreme ultraviolet reflectometry near resonance edges, Appl. Opt. 54 (35) (2015) 10351, , https://doi.org/10.1364/AO.54.010351.

[7] I. Balasa, X. Neiers, M. Mende, L. Jensen, D. Ristau, Investigation of binary coating material mixtures using grazing incidence EUV-reflectometry, Proc. SPIE 9237 (2014) 92371Y, https://doi.org/10.1117/12.2068197.

[8] C. Peth, F. Barkusky, K. Mann, Near-edge x-ray absorption fine structure measurements using a laboratory-scale XUV source, J. Phys. D. Appl. Phys. 41 (10) (2008) 105202, , https://doi.org/10.1088/0022-3727/41/10/105202.

[9] E.O. Filatova, a.a. Sokolov, E.Y. Taracheva, I.V. Bagrov, Studying natural oxide on the surface of n-Si(111), n-Si(100), and p-Si(111) single crystal wafers by X-ray reflection spectroscopy, Tech. Phys. Lett. 35 (1) (2009) 70–72, https://doi.org/10.1134/S1063785009010210.

[10] M. Fernández-Perea, J.A. Méndez, J.A. Aznárez, J.I. Larruquert, In situ reflectance and optical constants of ion-beam-sputtered SiC films in the 58.4 to 149.2 nm region, Appl. Opt. 48 (24) (2009) 4698–4702, https://doi.org/10.1364/AO.48.004698.

[11] D. Garoli, F. Frassetto, G. Monaco, P. Nicolosi, M.-G. Pelizzo, F. Rigato, V. Rigato, A. Giglia, S. Nannarone, Reflectance measurements and optical constants in the extreme ultraviolet-vacuum ultraviolet regions for SiC with a different C/Si ratio, Appl. Opt. 45 (2006) 5642–5650, https://doi.org/10.1364/AO.45.005642.

[12] J.I. Larruquert, R.A.M. Keski-Kuha, Reflectance measurements and optical constants in the extreme ultraviolet for thin films of ion-beam deposited SiC, Mo, Mg_2Si, and InSb and of evaporated Cr, Appl. Opt. 39 (16) (2000) 2772–2781.

[13] C. Tarrio, R.N. Watts, T.B. Lucatorto, J.M. Slaughter, C.M. Falco, Optical constants of in situ-deposited films of important extreme-ultraviolet multilayer mirror materials, Appl. Opt. 37 (19) (1998) 4100–4104.

[14] E.O. Filatova, A.A. Sokolov, I.V. Kozhevnikov, E.Y. Taracheva, O.S. Grunsky, F. Schaefers, W. Braun, Investigation of the structure of thin HfO_2 films by soft x-ray reflectometry techniques, J. Phys. Condens. Matter 21 (18) (2009) 185012, , https://doi.org/10.1088/0953-8984/21/18/185012.

[15] D.G. Schlom, J.H. Haeni, A thermodynamic approach to selecting alternative gate dielectrics, MRS Bull. 27 (03) (2002) 198–204, https://doi.org/10.1557/mrs2002.71.

[16] Shu Yang, Sen Huang, Hongwei Chen, Chunhua Zhou, Qi Zhou, Michael Schnee, Qing-Tai Zhao, J. Schubert, K.J. Chen, AlGaN/GaN MISHEMTs with high-k $LaLuO_3$ gate dielectric, IEEE Electron Device Lett. 33 (7) (2012) 979–981, https://doi.org/10.1109/LED.2012.2195291.

[17] J. Schubert, O. Trithaveesak, W. Zander, M. Roeckerath, T. Heeg, H. Chen, C. Jia, P. Meuffels, Y. Jia, D. Schlom, Characterization of epitaxial lanthanum lutetium oxide thin films prepared by pulsed-laser deposition, Appl. Phys. A 90 (3) (2008) 577–579, https://doi.org/10.1007/s00339-007-4327-8.

[18] J.M.J. Lopes, M. Roeckerath, T. Heeg, E. Rije, J. Schubert, S. Mantl, V.V. Afanas'Ev, S. Shamuilia, A. Stesmans, Y. Jia, D.G. Schlom, Amorphous lanthanum lutetium oxide thin films as an alternative high-k gate dielectric, Appl. Phys. Lett. 89 (22) (2006) 10–13, https://doi.org/10.1063/1.2393156.

[19] Y. Liu, M. Xu, J. Heo, P.D. Ye, R.G. Gordon, Heteroepitaxy of single-crystal $LaLuO_3$ on GaAs(111)A by atomic layer deposition, Appl. Phys. Lett. 97 (16) (2010) 162910, , https://doi.org/10.1063/1.3504254.

[20] A. Schäfer, F. Wendt, S. Mantl, H. Hardtdegen, M. Mikulics, J. Schubert, M. Luysberg, A. Besmehn, G. Niu, T. Schroeder, Hexagonal $LaLuO_3$ as high-κ dielectric, J. Vacuum Sci. Technol. B Nanotechnol. Microelectron. 33 (1) (2015) 01A104, https://doi.org/10.1116/1.4904401.

[21] M. Bohr, R. Chau, T. Ghani, K. Mistry, The high-k solution, IEEE Spectr. 44 (10) (2007) 29–35, https://doi.org/10.1109/MSPEC.2007.4337663.

[22] A. Schäfer, Growth and Characterization of Crystalline Rare-Earth Based Thin Oxide Films for the Application as Gate Dielectric in Nanotechnology, Ph.D. thesis RWTH Aachen University, 2015.

[23] S. Nannarone, F. Borgatti, A. DeLuisa, B. Doyle, G. Gazzadi, A. Giglia, P. Finetti, N. Mahne, L. Pasquali, M. Pedio, G. Selvaggi, G. Naletto, M. Pelizzo, G. Tondello, The BEAR beamline at Elettra, AIP Conf. Proc. 705 (2004) 450–453, https://doi.org/10.1063/1.1757831.

[24] A.C. Thompson (Ed.), X-Ray Data Booklet, Lawrence Berkeley National Laboratory, Center for X-Ray Optics and Advanced Light Source, LBNL/PUB-490 rev.3, 2009.

[25] D.L. Windt, IMD - software for modeling the optical properties of multilayer films, Comput. Phys. 12 (4) (1998), https://doi.org/10.1063/1.168689.

[26] S.N. Yakunin, I.A. Makhotkin, K.V. Nikolaev, R.W.E. van de Kruijs, M.A. Chuev, F. Bijkerk, Combined EUV reflectance and X-ray reflectivity data analysis of periodic multilayer structures, Opt. Express 22 (17) (2014) 20076, , https://doi.org/10.1364/OE.22.020076.

[27] Y.O. Volkov, I.V. Kozhevnikov, B.S. Roshchin, E.O. Filatova, V.E. Asadchikov, Model approach to solving the inverse problem of X-ray reflectometry and its application to the study of the internal structure of hafnium oxide films, Crystallogr. Rep. 58 (1) (2013) 160–167, https://doi.org/10.1134/S1063774513010148.

[28] I.G. Hughes, T.P.A. Hase, Measurements and their Uncertainties. A Practical Guide to Modern Error Analysis, Oxford University Press, 2010.

[29] M. Born, E. Wolf, Principles of Optics, Cambridge University Press, Cambridge, 1999.

[30] G.A. Korn, T.M. Korn, Mathematical Handbook for Scientists and Engineers: Definitions, Theorems, and Formulas for Reference and Review, Dover Publications, 2000.

[31] M. Hofstetter, A. Aquila, M. Schultze, A. Guggenmos, S. Yang, E. Gullikson, M. Huth, B. Nickel, J. Gagnon, V.S. Yakovlev, E. Goulielmakis, F. Krausz, U. Kleineberg, Lanthanum-molybdenum multilayer mirrors for attosecond pulses between 80 and 130 eV, New J. Phys. 13 (2011), https://doi.org/10.1088/1367-2630/13/6/063038.

[32] B. Henke, E. Gullikson, J. Davis, X-ray interactions: Photoabsorption, scattering,

transmission, and reflection at E = 50–30 000 eV, Z = 1–92, At. Data Nucl. Data Tables 54 (2) (1993) 181–342, https://doi.org/10.1006/adnd.1993.1013.
[33] Y. Uspenskii, J. Seely, N. Popov, I. Artioukov, A. Vinogradov, D. Windt, B. Kjornrattanawanich, Extreme UV optical constants of rare-earth metals free from effects of air contamination, Proc. SPIE, Soft X-Ray Lasers and Applications VI, 5919 2005, https://doi.org/10.1117/12.620042.
[34] J. Chen, E. Louis, C.J. Lee, H. Wormeester, R. Kunze, H. Schmidt, D. Schneider, R. Moors, W. van Schaik, M. Lubomska, F. Bijkerk, Detection and characterization of carbon contamination on EUV multilayer mirrors, Opt. Express 17 (19) (2009) 16969–16979, https://doi.org/10.1364/OE.17.016969.
[35] J. Hollenshead, L. Klebanoff, Modeling radiation-induced carbon contamination of extreme ultraviolet optics, J. Vacuum Sci. Technol. B 24 (1) (2006) 64, https://doi.org/10.1116/1.2140005.
[36] K.L. Ovanesyan, a.G. Petrosyan, G.O. Shirinyan, C. Pedrini, L. Zhang, Single crystal growth and characterization of LaLuO3, Opt. Mater. 10 (September) (1998) 291–295, https://doi.org/10.1016/S0925-3467(98)00008-1.
[37] M. Björck, G. Andersson, GenX: an extensible X-ray reflectivity refinement program utilizing differential evolution, J. Appl. Crystallogr. 40 (6) (2007) 1174–1178, https://doi.org/10.1107/S0021889807045086.
[38] L. Névot, P. Croce, Caractérisation des surfaces par réflexion rasante de rayons X. Application à l'étude du polissage de quelques verres silicates, Rev. Phys. Appl. 15 (3) (1980) 761–779, https://doi.org/10.1051/rphysap:01980001503076100.